Size-Dependent Strain Relaxation and Optical Characteristics of InGaN/GaN Nanorod LEDs

Yuh-Renn Wu, *Member, IEEE*, Chinghua Chiu, Cheng-Yu Chang, *Student Member, IEEE*,
Peichen Yu, *Member, IEEE*, and Hao-Chung Kuo, *Senior Member, IEEE*

***Abstract*—In this paper, InGaN/GaN nanorod LEDs with various sizes are fabricated using self-assembled Ni nanomasks and inductively coupled plasma-reactive ion etching. Photoluminescence (PL) characteristics exhibit size-dependent, wavelength blue shifts of the emission spectra from the nanorod LEDs. Numerical analyses using a valence force field model and a self-consistent Poisson, Schrödinger, and drift-diffusion solver quantitatively describe the correlation between the wavelength blue shifts and the strain relaxation of multiple quantum wells embedded in nanorods with different averaged sizes. Time-resolved PL studies confirm that the array with a smaller size exhibits a shorter carrier lifetime at low temperature, giving rise to a stronger PL intensity. However, the PL intensity deteriorates at room temperature, compared to that of a larger size, possibly due to an increased number of surface states, which decreases the nonradiative lifetime, and hence reduces the internal quantum efficiency.**

***Index Terms*—LEDs, nanotechnology.**

I. Introduction

III-NITRIDES have become prominent materials for optoelectronic devices and high power electronics [1]–[6]. The bandgaps of III-nitride alloys are continuously tunable from 6.2 to 0.7 eV, which covers the entire UV to near infrared spectrum. The wide direct bandgap property makes III-nitrides particularly promising for UV and blue LEDs. Moreover, it is also possible to convert the UV and blue into green and red light for white light sources with the assistance of phosphors. However, due to the large lattice mismatch $\sim$10% between InN and GaN for crystal growth along the c-axis, the InGaN/GaN multiple quantum wells (MQWs) suffer an epitaxially induced strain, leading to a strong piezoelectric field inside the wells, and worsening the crystalline quality. The resulting quantum-confined Stark effect (QCSE) further limits the internal quantum efficiency of InGaN/GaN MQW LEDs. Recently, the advances in nanofabrication technologies have allowed the fabrication of GaN-based nanostructures [7]–[11], posing a viable solution to relieving the strain in MQWs using nanostructured LEDs and potentially pushing to longer emission wavelengths with higher compositions of indium. Multiple studies have also been made on optical properties of the GaN-based nanostructures [10], [12]. In our recent work, we have demonstrated a single, free-standing GaN-based nanorod with a diameter of 300 nm using the focused ion beam (FIB) technique [12]. The microphotoluminescence (μ-PL) from the embedded GaN/InGaN MQWs reveals an energy blue shift of 68.3 meV contributed by the strain relaxation in MQWs. Still, few reports had yet been made for the size-dependent, strain relaxation effects on the emission characteristics, In this study, InGaN/GaN nanorod LEDs with a height of $\sim$700 nm and averaged sizes ranging from 120 to 300 nm are fabricated using self-assembled Ni clusters as the etch masks and inductively coupled plasma–reactive ion etching (ICP-RIE). Both frequency- and time-resolved PL(TRPL) characterizations are performed to analyze the size-dependent emission characteristics. Furthermore, a valence force field (VFF) model is developed to study the strain relaxation properties of InGaN/GaN MQWs embedded in the nanorod structures. The strain distribution and strain-induced polarization effect inside the MQWs is added to our self-consistent Poisson, drift-diffusion, and Schrödinger solver to analyze the emission characteristics in details. The emission spectra from nanorod LEDs of various sizes and under different carrier injection conditions are calculated, where reasonable agreements with the experimental results are obtained.

II. Fabrication

As illustrated in Fig. 1, the GaN nanorod LEDs of different averaged sizes were fabricated by a relatively simple method, using self-assembled Ni nanoclusters as the etch masks and ICP-RIE process. The samples were grown by metal–organic chemical vapor deposition (MOCVD) with a rotating-disk reactor on a c-plane sapphire (0 0 0 1) substrate at a growth pressure of 200 mbar. The epitaxial structure consisted of a 30-nm-thick GaN nucleation layer, a 2-μm-thick unintentionally doped GaN buffer layer, a 2-μm-thick Si-doped n-GaN layer, an unintentionally doped InGaN/GaN MQW active region, and a 0.2-μm-thick Mg-doped p-GaN. The MQW active region consists of ten pairs of 3- and 7-nm-thick InGaN wells and GaN barriers.

Fig. 1 illustrates the fabrication process of the nanorod LEDs with embedded InGAN/GaN MQWs. Based on our previous experimental results, a thin metal film can be self-assembled into nanoscaled islands after rapid temperature annealing (RTA), and the metal islands can result in better distribution

Manuscript received December 1, 2008; revised February 5, 2009. First published March 6, 2009; current version published August 5, 2009. This study was supported in part by National Science Council, Taiwan, under Grants 97-2221-E-002-050, 97-2623-7-002-018-ET, 96-2221-E-009-095-MY3, and in part by the Ministry of Economic Affairs (MOEA) project under Contract 95-EC-17-A-07-S1-011.

Y.-R. Wu and C.-Y. Chang are with the Graduate Institute of Photonics and Optoelectronics and the Department of Electrical Engineering, National Taiwan University, Taipei 10617, Taiwan (e-mail: yrwu@cc.ee.ntu.edu.tw; r96941079@ntu.edu.tw).

C. Chiu, P. Yu, and H.-C. Kuo are with the Department of Photonics and Institute of Electro-Optical Engineering, National Chiao Tung University (NCTU), Hsinchu 300, Taiwan (e-mail: chchiu.eo95g@nctu.edu.tw; yup@faculty.nctu.edu.tw; hckuo@faculty.nctu.edu.tw).

Color versions of one or more of the figures in this paper are available online at http://ieeexplore.ieee.org.

Digital Object Identifier 10.1109/JSTQE.2009.2015583

1077-260X/$25.00 © 2009 IEEE

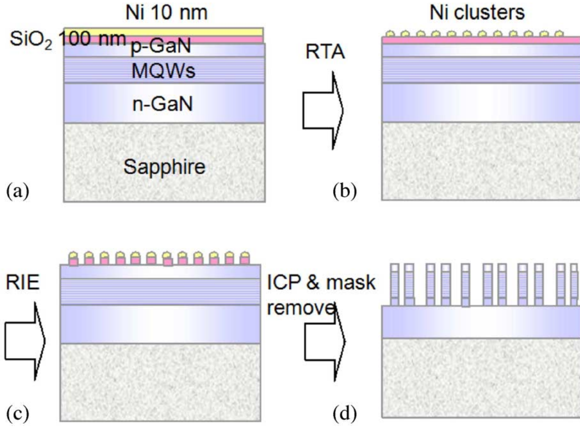

Fig. 1. Fabrication processes of nanorod LED arrays.

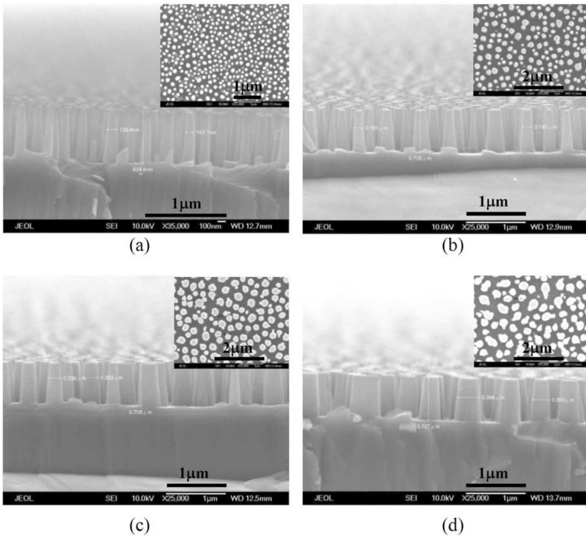

Fig. 2. Cross-sectional, SEMs of the fabricated GaN nanorod LEDs. The averaged diameters from (a) to (d) are 120, 180, 220, and 300 nm, respectively. The corresponding insets show the top view images of Ni-nanoscaled islands.

uniformity with a dielectric film deposited underneath the metal layer. Therefore, a 100-nm-thick SiO_2 layer was first deposited on the epi-surface of LEDs by plasma-enhanced chemical vapor deposition (PECVD). Then, an Ni film with various thicknesses of 5, 10, 15, and 20 nm was evaporated on SiO_2 layer using an electron beam evaporating system [Fig. 1(a)], followed by the RTA process with an N_2 flow rate of 10 SCCM at 850 for 90 s to form Ni nanoclusters, serving as the etching masks [Fig. 1(b)]. Since the RTA environments were identical for all the four samples, the different Ni thicknesses result in different averaged diameters and densities of the nanoclusters. Hence, the nanorod LEDs with various sizes could be fabricated. All samples with Ni nanomasks were subsequently performed using RIE and ICP to transfer the nanoscaled pattern into the SiO_2 layer [Fig. 1(c)] and GaN under the same etching condition. Finally, remove both the Ni metal masks and SiO_2 in heated nitric acid and buffered oxide etchant (BOE) [Fig. 1(d)]. Details of the nanomasks formation process were described in [13].

Fig. 2(a)–(d) shows the cross-sectional, SEMs of the fabricated GaN nanorod LEDs. The corresponding insets show the top view images of Ni-nanoscaled islands fabricated with metal thicknesses of 5, 10, 15, and 20 nm. From these images, all fabricated nanorod LEDs have a nearly identical height of $\sim$700 nm. The averaged diameters were $\sim 120 \pm 20$, 180 ± 20, 220 ± 20, and 300 ± 30 nm with densities decreasing from 3×10^9 to 5×10^8 cm^{-2}.

III. Theoretical Model

In order to analyze the correlation between the strain relation and emission characteristics, the VFF model [12], [14], [15] is developed to calculate the strain distribution of the nanorod LEDs. The VFF model is a microscopic model, where the interactions between each atom and its nearby atoms are considered. The total elastic energy is expressed as a function of atomic positions $\vec{R}_i$ using the summation of bond stretching (V_2) and bond bending (V_3) terms

$$\begin{aligned} E_{AE} &= \sum_{ij} V_2(\vec{R}_i - \vec{R}_j) + \sum_{ijk} V_3(\hat{\theta}_{ijk}) \\ &= \frac{1}{2}\sum_i \sum_j^{nn} \frac{3\alpha_{ijk}}{8(d_{ij}^0)^2}\left[(\vec{R}_i - \vec{R}_j)^2 - \left(d_{ij}^0\right)^2\right]^2 \\ &\quad + \frac{1}{2}\sum_i \sum_{j,k>j}^{nn} \frac{3\beta_{ijk}}{8d_{ij}^0 d_{ij}^0}\left[(\vec{R}_j - \vec{R}_i)\cdot(\vec{R}_k - \vec{R}_i)\right. \\ &\quad \left. - \cos\,\theta_0 d_{ij}^0 d_{ij}^0\right]^2 \end{aligned} \tag{1}$$

where d_{ij}^0 denotes the unstrained bond length between atoms i and j, and θ_0 is the unstrained bond angle, and $\cos\,\theta_0 = -1/3$. The bond stretching α and bond bending β force constants are listed in Mattila and Zunger [14]. The strain energy of each atom is minimized by an iterative method to find the most stable configuration. Once the system reaches the lowest energy, the strain distribution inside the structure can be obtained.

After obtained the strain distribution of the QW inside the nanorod structure, we can obtain the piezoelectric polarization induced by the strain, expressed as

$$P_{ez} = e_{31}\left(\epsilon_{xx} + \epsilon_{yy}\right) + e_{33}\epsilon_{zz} \tag{2}$$

where e_{31} and e_{33} are the piezoelectric coefficients and can be found in Ambacher *et al.* [16]. After obtaining the piezoelectric polarization, the fixed polar charge density can be obtained from the difference of the piezoelectric and spontaneous polarization field.

Since P_{ez} is a distribution function of x, y, and z, we can calculate the piezoelectric polarization-induced charge densities of each unit cell by

$$\rho_{pz}(x,y,z) = \frac{P_{ez}(x,y,z+dz) - P_{ez}(x,y,z)}{dz}. \tag{3}$$

The calculated distribution of the polar charges inside the MQW is then used in the self-consistent Poisson, Schrödinger, and drift-diffusion solver developed in our lab [17] to calculate the band diagram, the emission spectrum, and the emission intensity under different charge conditions. Since all of our simulation results are from the PL measurement, in order to accurately model the band structure after light absorption from the laser

light source, we also apply a generation term in the continuity equation (drift-diffusion) to model the carriers generated from light absorption, expressed as

$$\nabla \vec{J}_{n,p} = q(G - R) \quad (4)$$

where R is the carrier recombination rate from either radiative channel or nonradiative channel; G is the carrier generation term and depends on the excitation strength and the material absorption coefficient. The emission rate of MQWs inside the nanorod can be expressed as [18]

$$R_{spon} = \int d(\hbar\omega) \frac{e^2 n_r \hbar\omega}{m_0^2 \varepsilon_0 c^3 \hbar^2} \sum_{i,j} \int \frac{2}{(2\pi)^2} d\mathbf{k} \left|\hat{a} \cdot \mathbf{p_{i,j}}\right|^2 \times \frac{1}{\sqrt{2\pi}\sigma} \exp\left(\frac{-(E_{i,j} - \hbar\omega)^2}{2\sigma^2}\right) f^e f^h \quad (5)$$

where $E_{i,j}$ is the averaged energy separation between the electron state i and hole state j, n_r is the refractive index, and σ is the inhomogeneous broadening factor. $f^e(\mathbf{k})$ and $f^h(\mathbf{k})$ are the Fermi–Dirac distribution of electrons and holes, respectively. $|\hat{a} \cdot \mathbf{p_{i,j}}|^2$ is the momentum matrix element between the electron state, i, and the hole state, j. With the electronic band structures and the energy states obtained from the self-consistent solver, we can apply (5) to study the relative intensity of the emission spectrum, wavelength shift, and the screen and band-filling effects at various carrier injection conditions.

IV. Results and Discussion

Fig. 3(a) and (b) shows the measured PL from a regular LED and nanorod LEDs with various average diameters at low temperature 20K and room temperature, respectively. The pumping powers for all measurements are 15 mW at a laser spot size of 200 μm. As shown in Fig. 3(a), as the averaged rod diameter becomes smaller, the emission peak shows a clear blue shift. The PL intensity is strongest for LEDs with the smallest averaged diameter, 120 nm. The intensity decreases as the diameter becomes larger. However, the PL characteristics at room temperature are slightly different from those at the low temperature 20 K. First, the emission peak still has a clear blue shift as the diameter becomes smaller. Second, the PL intensity is strongest for LEDs with an averaged diameter of 220 nm. PL intensities are deteriorated at room temperature for nanorod LEDs of 120 and 180 nm. The PL intensity of the regular LED is much weaker than nanorod LEDs due to a stronger QCSE and lower light extraction efficiency. Fig. 4 shows the peak energy shift versus the rod diameters. The PL peak position of the regular LED is also plotted as the reference point. We can find that the fitted slopes at room temperature and 20 K are around 17.047 and 16.323 eV·nm, respectively.

The changes in PL intensity could be due to the absorption of excitation, the emission volume, light extraction efficiency, and defect densities of the nanorod LEDs. Therefore, it is hard to quantitatively analyze the size-dependent characteristics of the PL intensity and we will discuss qualitatively later. On the other hand, the blue shift of the spectrum is large (>100 meV) and cannot be simply explained by the band-filling effect or the carrier screening of QCSE. In particular, the power density of PL is not strong enough to induce a very high carrier density in the MQWs. The other possibility is the strain relaxation of the QW [12]. For InGaN/GaN, QW structures grown along c-axis, there exists a strong strain-induced piezoelectric polarization field inside the device. This will contribute to the band bending and red shift of spectrum, known as the QCSE. For the QW structure at the edge of nanorod surface, the lateral confinement of the QW is weak such that the relaxation of the InGaN QW layer is possible. The relaxed strain reduces the piezoelectric field inside the QW so that the spectrum shows a blue shift of the

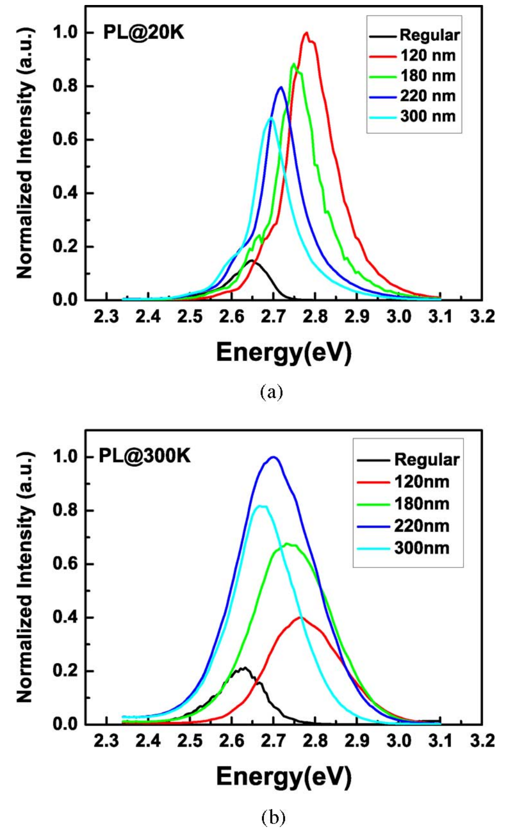

Fig. 3. PL spectra of a regular LED and nanorod LED arrays with different sizes at (a) 20 K and (b) room temperature.

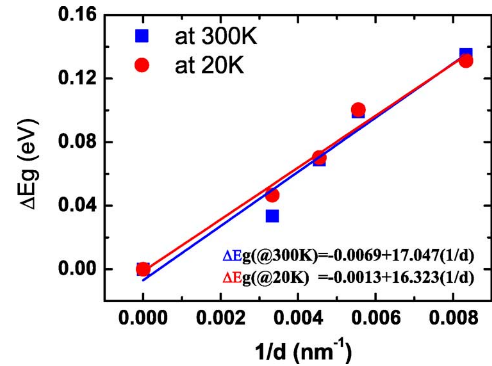

Fig. 4. Measured peak shift and fitted curve versus nanorod diameters at room temperature and at 20 K.

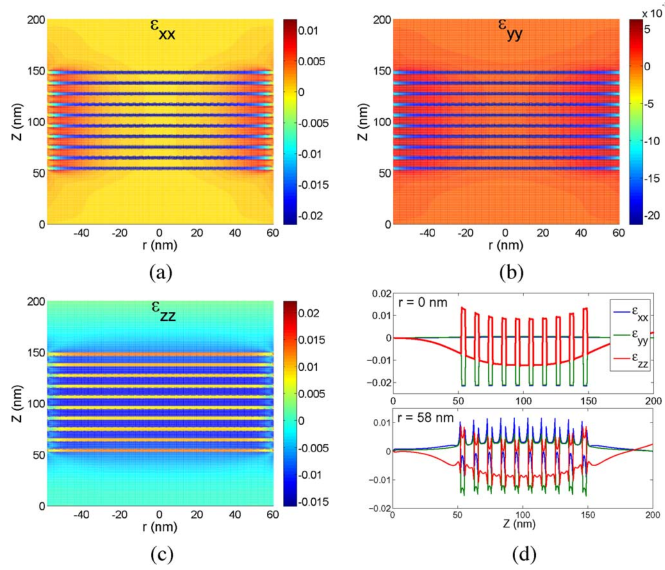

Fig. 5. Calculated strain distributions of $In_{0.2}Ga_{0.8}N$/GaN MQWs embedded in a free-standing, cylindrical-shaped nanorod with a height of $Z = 200$ nm and a width of $d = 120$ nm for (a) in-plane strain tensor ε_{xx} and (b) in-plane strain tensor ε_{yy}, (c) vertical strain tensor ε_{zz}, and (d) 2-D plots of strain tensors at the center and at the edge of the nanorod.

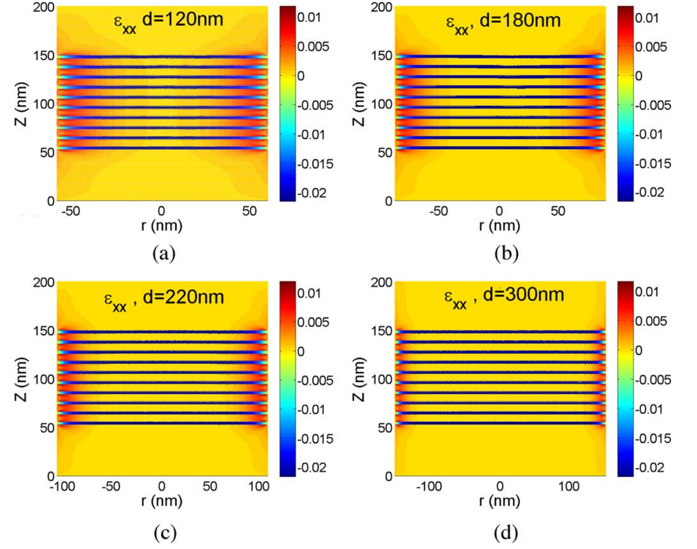

Fig. 6. Calculated strain ϵ_{xx} for nanorod LEDs with various averaged diameters. (a) 120 nm. (b) 180 nm. (c) 220 nm. (d) 300 nm.

emission wavelength. This blue shift should be observed for low-power, high-power, low-temperature, and room-temperature PL measurements.

In order to confirm the observed wavelength blue shift, we first apply the VFF model described in (1) in the previous section. Once the atoms' positions are known, calculating the strain tensor distribution is straightforward. To maintain the symmetry in a wurtzite structure, free-standing, cylindrical-shaped GaN nanorods consisting of ten-pair $In_{0.2}Ga_{0.8}N$ MQWs are defined with various diameters ranging from 120 to 300 nm. The nanorod has a fixed boundary condition at the bottom and free boundary conditions on other sides. Fig. 5 shows the calculated strain distribution for the nanorod with a diameter equal to 120 nm. Fig. 5(a)–(c) shows the strain tensor ε_{xx}, ε_{yy}, and ε_{zz} of the cross section of $x - z$ plane at the center of y-axis, respectively. Fig. 5(d) shows the line plot at $r = 58$ nm and $r = 0$ nm (center) of strain tensor. Both strain tensors show considerable relaxations on the outer shell of the nanorod, and as-grown-like strain distributions in the center of the nanorod. As shown in Fig. 5(a), the strain relaxation of ε_{xx} occurs at a distance of 20 nm from the edge of the nanorod. At $r = 58$ nm, where the change of strain from the nanorod center is most significant, there exist substantial strain variations on the QW/barrier interfaces and a slight tensile strain of ε_{xx} in the barriers. There is also a slight strain relaxation of ϵ_{yy} due to the circular shape of the rod. We also observe a vertical distribution of ε_{zz} in the Z-direction, mainly arising from the stacking of MQWs.

Fig. 6(a)–(d) shows the strain tensors ϵ_{xx} for nanorod diameters equal to 120, 180, 220, and 300 nm, respectively. As shown in Fig. 6, the major strain relaxation region is limited to 20 nm from the edge, regardless of the rod diameters. Therefore, the ratio of strain-relaxed MQW region to the strained region size becomes larger as the diameter decreases. With the calculated strain information, it is possible to calculate the emission spectra of nanorod LEDs with different sizes. Both in-plane and vertical strain tensors contribute to the polarization field and can be calculated by (2). Based on the calculated strain, as shown in Fig. 5, and the induced polarization charge calculated by (3). The calculated results are subsequently inserted into the self-consistent Poisson, Schrödinger, and drift-diffusion solver to calculate the band structure of the MQWs. The parameters needed for the band structure calculation can be found in Ambacher *et al.* [16].

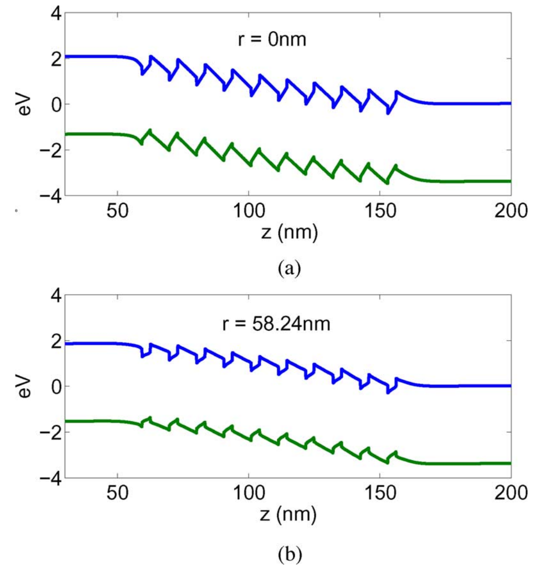

Fig. 7. Calculated conduction and valence band profiles of the MQWs embedded in a nanorod with a diameter of 120 nm at (a) center ($r = 0$ nm) and (b) edge ($r = 58.24$ nm) of the nanorod.

Fig. 7 shows the calculated band structures of the ten-pair MQW structure for different strain conditions: (a) at the center and (b) at the edge of the nanorod with a diameter of 120 nm.

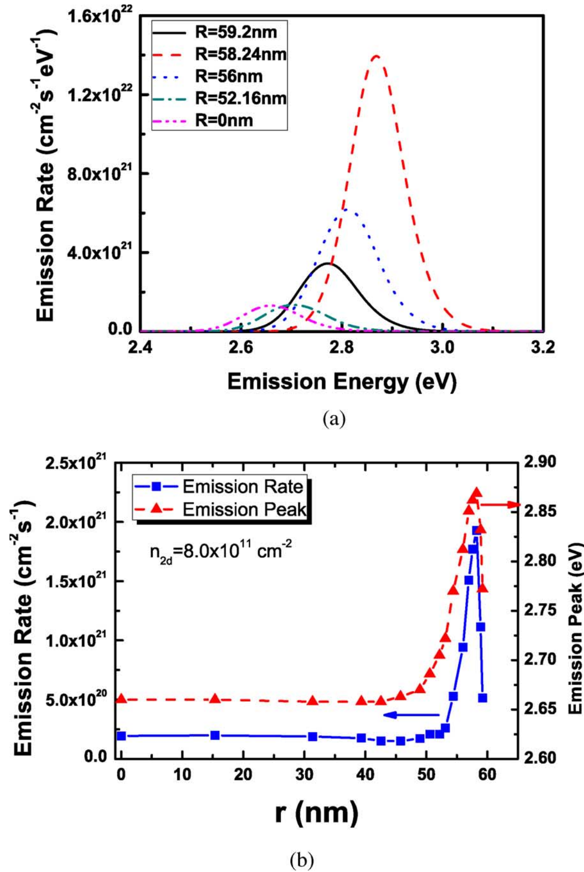

Fig. 8. (a) Calculated spontaneous emission rates as a function of emission energy at different positions of the nanorod with a diameter of 120 nm under the injected electron density at 8×10^{11} cm^{-2}. (b) Calculated spectrum peak shift and emission rates from the center to the edge of the nanorod.

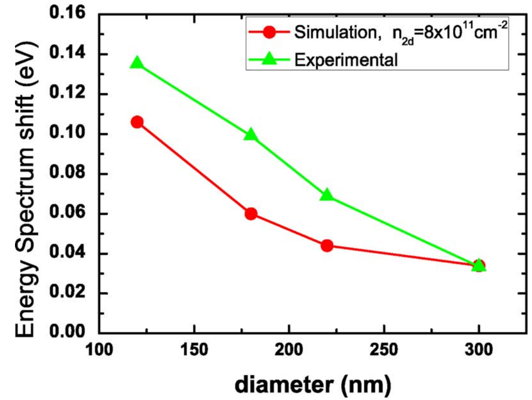

Fig. 9. Measured and calculated emission peak shift versus the nanorod diameters.

The polarization charge density induced by strain is taken into account as a function of the depth and the spontaneous polarization. As shown in Fig. 7, the band bending at the center of the nanorod is the strongest while the band bending at the edge is the weakest at $r = 58$ nm, where the strain relaxation reaches the maximum. In order to compare the PL intensity and compare the energy shift of the emission peak at different regions, we use the eigenfunctions and eigen levels obtained from (5) to calculate the emission intensity and the energy shift. The calculated results are shown in Fig. 8.

Fig. 8(a) shows the calculated emission spectra of the MQW structure at different regions of the nanorod structure with a diameter of 120 nm and under an injected electron density of 8×10^{11} cm^{-2} ($n_{\rm 3d} \sim 2.7 \times 10^{18}$ cm^{-3}). The average hole density is around 7×10^{12} cm^{-2}, which is much higher than electron density due to the heavier effective mass and smaller diffusion length so that more holes stay inside the QW after electron–hole pairs are generated. As shown in Fig. 8(a), the emission intensity near the edge is the strongest. For $r < 45$ nm, the emission strength does not change much, and this can be explained by the insignificant strain variation from the center, as shown in Fig. 5. Moreover, Fig. 8(b) shows the calculated emission peak shift and emission rates as a function of the radius of the cylindrical nanorod under an injected electron density of 8×10^{11} cm^{-2}. The maximum emission peak shift occurs at $r = 58$ nm where 200 meV blue shift is achieved, compared to the emission from center of the nanorod. At $r = 60$ nm, the strain relaxation is not the maximum at the surface so that the energy shift maximum does not occur here. The emission rate reaches the maximum at edge and decreases rapidly from $r = 60$ nm to $r = 45$ nm. The emission rates are almost constants for $r < 45$ nm, where the electron–hole wavefunction overlap does not change too much here. Since the center of MQWs are still suffered from the strain with its magnitude comparable to that of the as-grown planar structure, the PL from the center of the nanorod contributes to the red-edge emission, which is partially overlapped with the PL from the strained region. Therefore, we believe that the majority of the nanorod PL blue shift originates from the strain-relaxed region, within a distance of ∼15 nm near the edge of the nanorod, as shown in Fig.8 (b). Moreover, the variation of strain tensors in the relaxation region results in a spatially varied polarization field, leading to a broadened emission spectrum.

The overall emission spectrum (in (electron volts·seconds) inverse) of the nanorod LEDs can be calculated by summing the emission spectra from different regions, which equivalently can be obtained by

$$R_{sp,\rm total}(\hbar\omega) = \int_0^{d/2} R_{sp}(\hbar\omega, r) 2\pi r \, dr \qquad (6)$$

where d is the diameter of the nanorod and r is the distance to the center of the nanorod. The $R_{sp}(\hbar\omega, r)$ is already obtained, as shown in Fig. 8(b). Fig. 9 shows the comparison between calculated emission peak from (6) and experimental measurement. We find the calculated size-dependent peak shift is well-agreed with the measurements. Our calculation results show that the blue shift mainly arises from the edge strain relaxation of the MQWs. Therefore, for the larger diameter nanorods, the volume ratio of the strain-relaxed region to the strained region becomes smaller so that the blue shift also becomes smaller.

As mentioned earlier, the PL intensity of the nanorod with the smallest diameters is the strongest at low temperature. However, at room temperature, the PL intensity maximum occurs for nanorod LEDs with an average diameter of 220 nm. The effects of extraction and absorption may be neglected since they

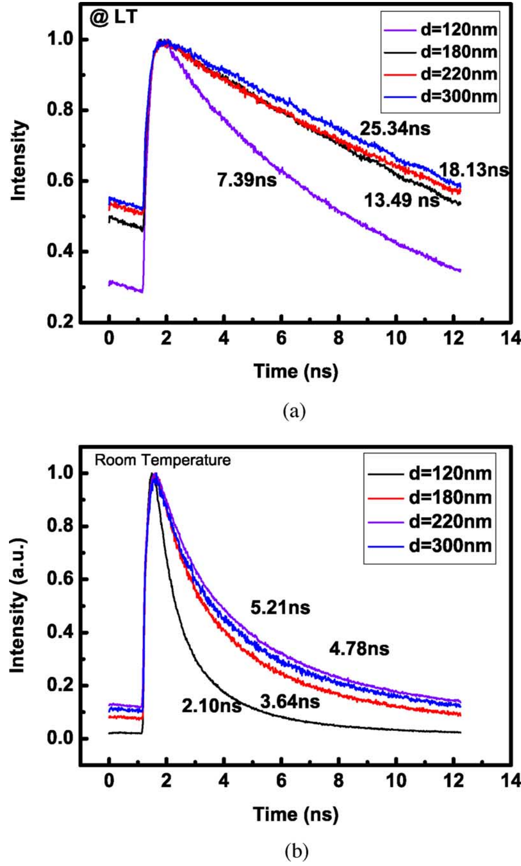

Fig. 10. (a) TRPL for nanorod LEDs with different sizes at 20 K. (b) TRPL for nanorod LEDs with different sizes at room temperature.

were measured from the same samples only at different temperatures. It is possible that the defect density contributes to the decease of the PL intensity. Therefore, we conduct the TRPL for both cases. Fig. 10(a) and (b) shows the measured TRPL at low temperature 20 K and room temperature, respectively. As shown in Fig. 10(a), the fitted decay times are 25.34, 18.13, 13.49, and 7.39 ns for nanorod diameters of 300, 220, 180, and 120 nm, respectively. The nanorod LEDs with the diameter of 120 nm have the smallest decay time. If the carrier decaying process is dominated by radiative recombination, the smallest diameter nanorod has the best efficiency. This can be also observed with the PL spectrum intensity, as shown in Fig. 3(a). However, at room temperature, we can find that the nanorod LEDs with the diameter of 220 nm have the strongest emission intensity. However, as shown in Fig. 10(b), the TRPL shows that the decay time of 120 nm nanorod has the smallest decay time. It is well-known that the PL decay lifetime is determined by both the radiative and nonradiative processes. If the radiative lifetime dominates, the emission intensity should be strongest for the smallest nanorod size due to the smallest decay time. However, the intensity of nanorod LEDs with a diameter of 120 nm exhibits an opposing behavior, as shown in Fig. 3(b). Hence, we conclude that the nonradiative decay process dominates and reduces the emission intensities at room temperature. The nanorod LEDs with a diameter size smaller than 180 nm

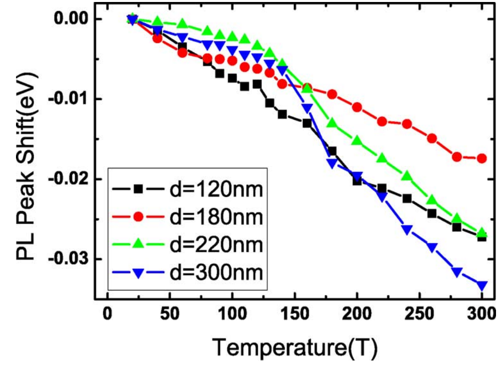

Fig. 11. Measured peak shifts as a function of temperature for nanorod LEDs with different sizes.

may have a large defect density. Although the nanorod LEDs with a small averaged diameter can increase the radiative recombination rate, the increased nonradiative recombination rate cancels the effect of radiative rate enhancement and limits the internal quantum efficiency.

Fig. 11 shows the energy peak shift versus temperature for nanorod LEDs with different diameters. In the temperature-dependent measurement, the bandgap shrinks as the temperature increases, giving rise to the red shift of the emission wavelength. Moreover, the freeze carriers also move rapidly, and hence are more likely to fall into localized states and then recombine. If the density of localized defect states is small, the defect states can be easily filled up. Therefore, the carriers can stay at band states, resulting in the reduction of red shift or even a small blue shift. As the temperature continues to increase, the red shift due to the bandgap shrinkage becomes dominant again and results in an s-curve for the emission peak shift. However, if the localized defect density is high, the localize states are less likely to be filled. The s-type emission peak shift therefore cannot be clearly observed. As shown in Fig. 11, the s-type peak shift is relatively obvious for nanorod LEDs with diameters of 300 and 220 nm. On the other hand, the s-curve is not as clear for those of 180 and 120 nm, indicating a considerable density of surface states. The temperature-dependent characteristics support our previous conclusion, suggesting the importance of surface passivation for nanorod LEDs with a small diameter.

V. Conclusion

In conclusion, we have demonstrated the size-dependent emission characteristics of InGaN/GaN MQW nanorod LEDs using both frequency-resolved PL and TRPL measurement at different temperatures. The strain distribution and the band profile of MQWs embedded in the nanorod structures are analyzed by the VFF model and the self-consistent solver. Our calculation shows that the energy shift and spectrum broadening could be strongly related to the strain relaxation at nanorod edge (~20 nm from the edge). The low-temperature PL measurements and calculations show that the nanorod LEDs with the smallest averaged diameter of 120 nm have the highest radiative recombination rate due to strain relaxation. However, as

the nanorod diameter becomes smaller than 200 nm, the nonradiative recombination at surface defects starts to affect the device performance at room temperature. As a result, the internal quantum efficiency is reduced. Therefore, surface passivation is critical for boosting efficiencies of strain-relaxed InGaN/GaN nanorod LEDs.

ACKNOWLEDGMENT

The authors would like to thank Prof. T. C. Lu at National Chiao Tung University (NCTU) for discussions of this study.

REFERENCES

[1] J. H. Chen, Z. C. Feng, H. L. Tsai, J. R. Yang, P. Li, C. Wetzel, T. Detchprohm, and J. Nelson, "Optical and structural properties of InGaN/GaN multiple quantum well structure grown by metalorganic chemical vapor deposition," *Thin Solid Films*, vol. 498, no. 1–2, pp. 123–127, 2006.

[2] W. K. Wang, D. S. Wuu, S. H. Lin, P. Han, R. H. Horng, T. C. Hsu, D. T. C. Huo, M. J. Jou, Y. H. Yu, and A. K. Lin, "Efficiency improvement of near-ultraviolet ingan leds using patterned sapphire substrates," *IEEE J. Quantum Electron.*, vol. 41, no. 11, pp. 1403–1409, Nov. 2005.

[3] C. C. Yu, C. F. Chu, J. Y. Tsai, H. W. Huang, T. H. Hsueh, C. F. Lin, and S. C. Wang, "Gallium nitride nanorods fabricated by inductively coupled plasma reactive ion etching," *Jpn. J. Appl. Phys. 2, Lett.*, vol. 41, no. 8B, pp. L910–L912, 2002.

[4] C. H. Chen, S. J. Chang, Y. K. Su, G. C. Chi, J. K. Sheu, and J. F. Chen, "High-efficiency InGaN-GaN MQW green light-emitting diodes with CART and DBR structures," *IEEE J. Sel. Topics Quantum Electron.*, vol. 8, no. 2, pp. 284–288, Mar./Apr. 2002.

[5] H. M. Kim, D. S. Kim, D. Y. Kim, T. W. Kang, Y. H. Cho, and K. S. Chung, "Growth and characterization of single-crystal GaN nanorods by hydride vapor phase epitaxy," *Appl. Phys. Lett.*, vol. 81, no. 12, pp. 2193–2195, 2002.

[6] S. Nakamura, "GaN-based blue/green semiconductor laser," *IEEE J. Sel. Topics Quantum Electron.*, vol. 3, no. 2, pp. 435–442, Apr. 1997.

[7] S. Han, W. Jin, D. H. Zhang, T. Tang, C. Li, X. L. Liu, Z. Q. Liu, B. Lei, and C. W. Zhou, "Photoconduction studies on GaN nanowire transistors under UV and polarized UV illumination," *Chem. Phys. Lett.*, vol. 389, no. 1–3, pp. 176–180, 2004.

[8] J. C. Johnson, H. J. Choi, K. P. Knutsen, R. D. Schaller, P. D. Yang, and R. J. Saykally, "Single gallium nitride nanowire lasers," *Nat. Mater.*, vol. 1, no. 2, pp. 106–110, 2002.

[9] M. S. Son, S. I. Im, Y. S. Park, C. M. Park, T. W. Kang, and K. H. Yoo, "Ultraviolet photodetector based on single GaN nanorod p–n junctions," *Mater. Sci. Eng. C-Biomimetic Supramol. Syst.*, vol. 26, no. 5–7, pp. 886–888, 2006.

[10] H. M. Kim, Y. H. Cho, H. Lee, S. I. Kim, S. R. Ryu, D. Y. Kim, T. W. Kang, and K. S. Chung, "High-brightness light emitting diodes using dislocation-free indium gallium nitride/gallium nitride multiquantum-well nanorod arrays," *Nano Lett.*, vol. 4, no. 6, pp. 1059–1062, 2004.

[11] W. Q. Han, S. S. Fan, Q. Q. Li, B. L. Gu, X. B. Zhang, and D. P. Yu, "Synthesis of silicon nitride nanorods using carbon nanotube as a template," *Appl. Phys. Lett.*, vol. 71, no. 16, pp. 2271–2273, 1997.

[12] P. Yu, C. H. Chiu, Y.-R. Wu, H. H. Yen, J. R. Chen, C. C. Kao, H.-W. Yang, H. C. Kuo, T. C. Lu, W. Y. Yeh, and S. C. Wang, "Strain relaxation induced microphotoluminescence characteristics of a single ingan-based nanopillar fabricated by focused ion beam milling," *Appl. Phys. Lett.*, vol. 93, no. 8, pp. 081110-1–081110-3, 2008.

[13] H. W. Huang, C. C. Kao, T. H. Hsueh, C. C. Yu, C. F. Lin, J. T. Chu, H. C. Kuo, and S. C. Wang, "Fabrication of GaN-based nanorod light emitting diodes using self-assemble nickel nano-mask and inductively coupled plasma reactive ion etching," *Mater. Sci. Eng. B*, vol. 113, pp. 125–129, 2004.

[14] T. Mattila and A. Zunger, "Predicted bond length variation in wurtzite and zinc-blende InGaN and AlGaN alloys," *J. Appl. Phys.*, vol. 85, no. 1, pp. 160–167, Jan. 1999.

[15] Y.-R. Wu, Y.-Y. Lin, H.-H. Huang, and J. Singh, "Electronic and optical properties of InGaN quantum dot based emitters for solid state lighting," *J. Appl. Phys.*, vol. 105, no. 2, pp. 013117-1–013117-7, 2009.

[16] O. Ambacher, J. Majewski, C. Miskys, A. Link, M. Hermann, M. Eickhoff, M. Stuzmann, F. Bernardini, V. Fiorentini, V. Tilak, B. Schaff, and L. F. Eastman, "Pyroelectric properties of Al(In)GaN/GaN hetero- and quantum well structures," *J. Phys.: Condens. Matter*, vol. 14, pp. 3399–3434, 2002.

[17] Y.-R. Wu, M. Singh, and J. Singh, "Gate leakage suppression and contact engineering in nitride heterostructures," *J. Appl. Phys.*, vol. 94, no. 9, pp. 5826–5831, Nov. 2003.

[18] H. Jiang, M. Minsky, S. Keller, E. Hu, J. Singh, and S. P. DenBaars, "Photoluminescence and photoluminescence excitation spectra of $In_{0.2}Ga_{0.8}N$/GaN quantum wells: Comparison between experimental and theoretical studies," *IEEE J. Quantum Electron.*, vol. 35, no. 10, pp. 1483–1490, Oct. 1999.

Yuh-Renn Wu (S'02–M'07) received the B.S. degree in physics and the M.S. degree in electrical engineering from National Taiwan University, Taipei, Taiwan, in 1998 and 2000, respectively, and the Ph.D. degree in electrical engineering from the Department of Electrical Engineering and Computer Science, University of Michigan, Ann Arbor, in 2006.

He is currently an Assistant Professor with the Graduate Institute of Photonics and Optoelectronic and Department of Electrical Engineering, National Taiwan University. He is currently engaged in physics, design of optoelectronic devices, and high power electronics. His current research interests include the studies of nitride-based quantum well, quantum wire, and quantum-dot LEDs, high-power and high-speed electronics, ferroelectrics, and optoelectronic devices.

Chinghua Chiu received the B.S. and M.S. degrees in the power mechanical engineering from National Tsing Hua University, Hsinchu, Taiwan, in 2004 and 2006, respectively. He is currently working toward the Ph.D. degree from the Department of Photonics, National Chiao Tung University (NCTU), Hsinchu.

His current research interests include the vertical LED and high-performance GaN-based LED via nanotechnology.

Cheng-Yu Chang (S'09) received the B.S. degree in the electrical engineering from National Central University, Jhongli, Taiwan, in 2007. He is currently working toward the M.S. degree from the Graduate Institute of Photonics and Optoelectronics and Department of Electrical Engineering, National Taiwan University, Taipei, Taiwan.

His current research interest includes device simulation on LEDs.

Peichen Yu (M'06) received the B.S. degree in electrophysics and the M.S. degree in electro-optical engineering from National Chiao Tung University (NCTU), Hsinchu, Taiwan, in 1996 and 1998, respectively, and the Ph.D. degree in electrical engineering from the University of Michigan, Ann Arbor, in 2004.

She worked as a design engineer for the Advanced Design Group, Intel Corporation, Hillsboro, OR, for two years, where she was engaged in OPC-related design rule definition and optical proximity correction (OPC) algorithm development of the diffusion layer for the CMOS 65 and 45 nm nodes. In August 2006, she joined the Department of Photonics, NCTU as an Assistant Professor. Her current research interests include the design and development of photonic crystal-based and quantum-dot-based semiconductor devices.

Hao-Chung Kuo (M'98–SM'06) received the B.S. degree in physics from National Taiwan University, Taipei, Taiwan, the M.S. degree in electrical and computer engineering from Rutgers University, New Brunswick, NJ, in 1995, and the Ph.D. degree from electrical and computer engineering department, University of Illinois at Urbana-Champaign, Urbana-Champaign, in 1999.

During 1993–1995, he was a Research Consultant in Lucent Technologies, Bell Laboratories. During 1999–2001, he was a Member of Technical Staff in Fiber-Optics Division, Agilent Technologies. During 2001–2002, he was a Member Technical Staff at LuxNet Corporation. Since October 2002, he has been a Faculty Member of the Institute of Electro-Optical Engineering, National Chiao Tung University (NCTU), Hsinchu, Taiwan, where he is currently the Associate Dean of the Office of International Affair, NCTU. His current research interests include semiconductor lasers, vertical-cavity surface-emitting lasers (VCSELs), blue and UV LED lasers, quantum-confined optoelectronic structures, optoelectronic materials, and solar cell. He has authored or coauthored 140 internal journal papers, and six granted and ten pending patents.

Prof. Kuo is the Institute of Electrical and Electronics Engineers (IEEE) Senior Member and Associate Editor of IEEE/OSA JOURNAL OF LIGHTWAVE TECHNOLOGY and IEEE Journal of Selected Topics in Quantum Electronics IEEE JOURNAL OF SELECTED TOPICS IN QUANTUM ELECTRONICS (special issue on Solid State Lighting). He received Ta-You Wu Young Scholar Award from National Science Council and Young Photonics researcher award in 2007.